Polymer Degradation and Stability 151 (2018) 80–89

Contents lists available at ScienceDirect

Polymer Degradation and Stability

journal homepage: www.elsevier.com/locate/polydegstab

Transparent and soluble polyimide films from 1,4:3,6-dianhydro-D-mannitol based dianhydride and diamines containing aromatic and semiaromatic units: Preparation, characterization, thermal and mechanical properties

Zhiming Mi[a], Zhixiao Liu[a], Jianan Yao[a], Chunbo Wang[a], Changjiang Zhou[b], Daming Wang[a], Xiaogang Zhao[a], Hongwei Zhou[a], Yumin Zhang[c], Chunhai Chen[a,*]

[a] Key Laboratory of High Performance Plastics (Jilin University), Ministry of Education, National & Local Joint Engineering Laboratory for Synthesis Technology of High Performance Polymer, College of Chemistry, Jilin University, Changchun, 130012, PR China
[b] State Key Laboratory of Supramolecular Structure and Materials, Jilin University, Changchun, 130012, PR China
[c] College of Chemistry, Jilin University, Changchun, 130012, PR China

ARTICLE INFO

Keywords:
1,4:3,6-dianhydrohexitol
Dianhydride
Polyimide
Structure-property relationships

ABSTRACT

To develop colorless and soluble polyimide films, a novel dianhydride containing 1,4:3,6-dianhydro-D-mannitol unit, 2,5-bis(3,4-dicarboxyphenoxy)-1,4:3,6-dianhydromannitol dianhydride (IMDA) was synthesized. And two series of polyimides were prepared *via* a two-step thermal imidization, PI－(1–4) were obtained from IMDA and four kinds of aromatic diamines while PI－(5–7) from IMDA and three kinds of semiaromatic diamines. All the polyimides were readily soluble in common polar solvents and could afford flexible, tough and colorless films with transparency up to 89% at 450 nm. Especially, polyimides simultaneously containing 1,4:3,6-dianhydrohexitol units in diamine and dianhydride exhibited comparable optical and soluble performance with the alicyclic fluorinated ones. Meanwhile, it was certified that 1,4:3,6-dianhydrohexitol fragment in dianhydride was more determinant in solubility and transmittance of polyimides than that in diamine. An overall investigation of these polyimides on thermal, mechanical, morphological, soluble, optical and dielectric properties was presented, and their structure-property relationships were discussed in detail.

1. Introduction

Colorless polymer films with high thermal stability and mechanical strength have been widely studied for applications in prospective flexible substrates of microelectronic and micro-optical devices in the field of displays, memory, lighting, solar cells, sensors and antennas etc. [1–4]. Among massive polymers, polyimides are one of the ideal candidates endowed with the outstanding thermal and mechanical properties, wide chemical resistance as well as relatively low dielectric constant [5]. Nonetheless, reddish-yellow coloration as well as difficulty in processability of aromatic polyimides should be taken into consideration before they can be suitable for optoelectronic applications [6].

Generally, the intra- and intermolecular charge-transfer (CT) interactions between the electron-donating diamine and electron-accepting aromatic dianhydride are considered as the main reason behind the deep yellow or reddish color of aromatic polyimides, and stiff and compact stacking of the molecular chains lead to the insolubility or infusibility of aromatic polyimides, which obstruct their processing and applications [7]. Classically, diamines or dianhydrides containing flexible or unsymmetrical linkages, ortho-methyl, noncoplanar structures, bulky trifluoromethyl substituents and aliphatic fragments were designed for the synthesis of polyimdes aiming at weakening several types of chain-chain interactions such as charge transfer formation, chain packing (e.g., crystallinity), and electronic polarization interactions [8,9]. Regrettably, in most cases, methodologies resulting in colorless and alleviated model proceeding difficulty of polymers usually inevitably deteriorated their thermal and mechanical properties at the same time, and vice versa [10]. Recently, cyclobutane, cyclohexane and cardo derived polyimides reached an ideal balance of these contradict goals [10], nevertheless, the synthesis of monomers, especially for dianhydrides, were often accompanied with harsh conditions like

* Corresponding author.
E-mail address: cch@jlu.edu.cn (C. Chen).

https://doi.org/10.1016/j.polymdegradstab.2018.01.006
Received 16 October 2017; Received in revised form 1 January 2018; Accepted 6 January 2018
Available online 09 January 2018
0141-3910/

photoirradiation and high-pressure oxidation with nitric acid or ozone, which implied synthetic difficulties, eco-unfriendly byproducts and high cost. And single modification either in diamine or dianhydride may be insufficient when these polyimides were subjected to strict requirements for optoelectronic performance [11]. Consequently, it was entirely justified to develop appropriate segments simultaneously contained in diamine and dianhydride, which may result in effective and convenient improvement of transparency and solubility of polyimides without significantly sacrificing their thermal and mechanical properties.

Of significant interest and extensively explored is the grain sourced alicyclic 1,4:3,6-dianhydrohexitols with three isomers (Fig. S1). Three structures including exo-endo, exo-exo and endo-endo oriented conformations are corresponding to 1,4:3,6-dianhydro-D-glucidol (isosorbide), 1,4:3,6-dianhydro-D-mannitol (isomannide) and 1,4:3,6-dianhydro-L-iditol (isoidide), respectively. Among these isomers, rare researches on isoidide were found due to its narrow origins [12]. Up to now, 1,4:3,6-dianhydrohexitols derived polyamide by Jasinska et al. [13], polycarbonate by Noordover et al. [14], polyurethanes by Marin et al. [15], and polyesters by Juais. et al. [16] and by Matuszowicz. et al. [17] have been intensively studied and some of them (e.g. DURABIO by Mitsui) have been industrialized production. However, reports about the incorporation of 1,4:3,6-dianhydrohexitol units into polyimide backbones were rare [18–20]. In our previous work, a series of diamines containing isosorbide segment were designed and polycondensed with commercial dianhydrides to achieve alicyclic fluorinated polyimides, and superior performance of those polyimides such as colorless and soluble properties were coefficient contribution of isosorbide fragment and bulky trifluoromethyl [19]. However, dianhydride containing 1,4:3,6-dianhydrohexitol units and its polycondensation with aromatic and semiaromatic diamines have not been reported, and the structure-property relationships of these polyimides retain to be explored.

In this paper, a novel dianhydride, 2,5-bis(3,4-dicarboxyphenoxy)-1,4:3,6-dianhydromannitol dianhydride (IMDA) was synthesized (Scheme 1) and two series of polyimides shown in Scheme 2 were prepared by the polycondensation of IMDA and aromatic diamines (a–d) and semiaromatic diamines (f–g), respectively. Characterizations including FTIR, HRLC-MS, ^{1}H, ^{13}C and 2D NMR spectra and elemental analysis were utilized to confirm the chemical structure of IMDA and polyimides. The combination of aromatic and semiaromatic diamines was aiming at clarifying the structure–property relationships of polyimides on morphology, solubility, thermal, mechanical, dielectric, and optical performance. The incorporation of 1,4:3,6-dianhydrohexitols (isosorbide and isomannide) into polyimides were in view of their intrinsic rigidity, alicyclic wedge-shaped structure, nontoxicity as well as biodegradability, and these five-membered alicyclic fragments were expected to simultaneously weaken the intermoleculer cohensive force and impede CT interactions to improve the transmittance and solubility of the polyimide films without compromising thermal and mechanical performance.

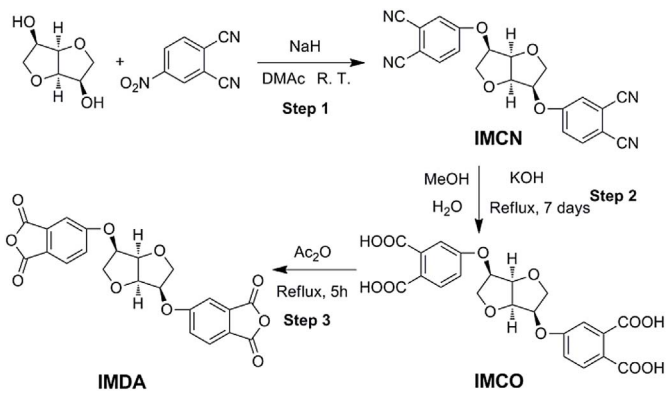

Scheme 1. Preparative route of monomers.

2. Experimental

2.1. Materials

P-phenylenediamine (a), 4,4′-oxydianiline (b), 4,4′-diaminobenzophenone (c) and 2,2-bis(4-aminophenyl)hexafluoropropane (d) were supplied by Tokyo Chemical Industry (TCI) and used as received. 2,5-Bis(4-amino-phenoxy)-1,4:3,6-dianhydrosorbitol (e), 2,5-bis(2-methyl-4-amino-phenoxy)-1,4:3,6-dianhydrosorbitol (f) and 2,5-bis(2-trifluoromethyl-4-amino-phenoxy)-1,4:3,6-dianhydrosorbitol (g) were synthesized accreting to our previously work [19]. Isomannide, 4-nitrophthalonitrile, methanol, sodium hydride and potassium hydroxide were purchased from Aldrich Chemical Co. and used as received. *N,N*-Dimethylformamide (DMF) and *N,N*-dimethylacetamide (DMAc) were purified by vacuum distillation over CaH_2 and stored over 4 Å molecular sieves prior to use. The other commercially available reagents and solvents were obtained from Sinopharm Chemical Reagent Beijing Co. Ltd. and used without further purification.

2.2. Characterization

FTIR spectra were performed using a Bruker Vector 22 spectrometer at a resolution of 4 cm^{-1} in the range of 400–4000 cm^{-1}. The ^{1}H NMR and ^{13}C NMR spectra were recorded on a BRUKER-300 spectrometer (300 MHz) using deuterated dimethylsulfoxide (dmso-d_6) as the solvent and tetramethylsilane (TMS) as the internal standard, and correlation spectra (COSY) and heteronuclear single quantum correlation (HSQC) were recorded on a BRUKER-AVANCEIII500 (500 MHz) at 300 K with technical specifications of ^{1}H S/N ≥ 760:1 (0.1% ethylbenzene in $CDCl_3$) and ^{13}C S/N > 500:1 (ASTM). The NMR data were processed using Topspin 3.2 software and all coupling constants were given in Hz and chemical shifts in ppm. Inherent viscosities (η_{inh}) of poly(amic acid) (PAA) solution were obtained with an Ubbelohde viscometer at 25 °C in DMAc at a concentration of 0.5 g dL^{-1}. Number average molecular weights (M_n) and weight average molecular weights (M_w) were measured *via* gel permeation chromatography (GPC) on the basis of polystyrene calibration on a PL-GPC 220 instrument equipped with a refractive index detector using DMF as an eluent at a flow rate of 1.0 mL/min, and the specification of GPC column was 3 × PLgel 10 μm; MIXED-B, 300 × 7.5 mm. High resolution liquid chromatography-mass spectrometry (HRLC-MS) data were recorded on an Agilent 1290-micrOTOF-QII instrument. Elemental analyses were conducted on a Vario EL cube CHN recorder elemental analysis instrument. Differential scanning calorimetric (DSC) analysis was conducted on a TA instrument DSC Q100 at a scanning rate of 10 °C/min under nitrogen, and the second heating scans were taken as the final data. Thermogravimetric analysis (TGA) was carried out on TA 2050 under air or nitrogen atmosphere with a heating rate of 10 °C/min. Dynamic mechanical analysis (DMA) was conducted on a TA instrument DMA Q800 with a load frequency of 1 Hz and a heating rate of 5 °C/min from room temperature to 350 °C in air, and the specimen was made with 10 mm width, 25 mm length, 45 μm thickness. Glass transition temperature (T_g) was determined as the peak temperature of tan δ curve. The coefficient of thermal expansion (CTE) was detected by thermomechanical analysis (TMA) on the polyimide film specimens (length, 10 mm; width, 5 mm; thickness, 45 μm) using a METTLER TMA/SDTA841^{e}. The measurement was carried out under N_2 with a heating rate of 10 °C/min at a load of 0.05 N during elongation. Mechanical properties were evaluated on a Shimadzu AG − I universal testing apparatus with a crosshead speed of 5 mm min^{-1}, and tensile strength (T_S), tensile modulus (T_M) and elongation at break (E_B) were calculated by the average of five strips (length, 25 mm; width, 10 mm; thickness, 45 μm). Wide-angle X-ray diffractometer (Empyrean, PANalytical B.V.) was equipped with

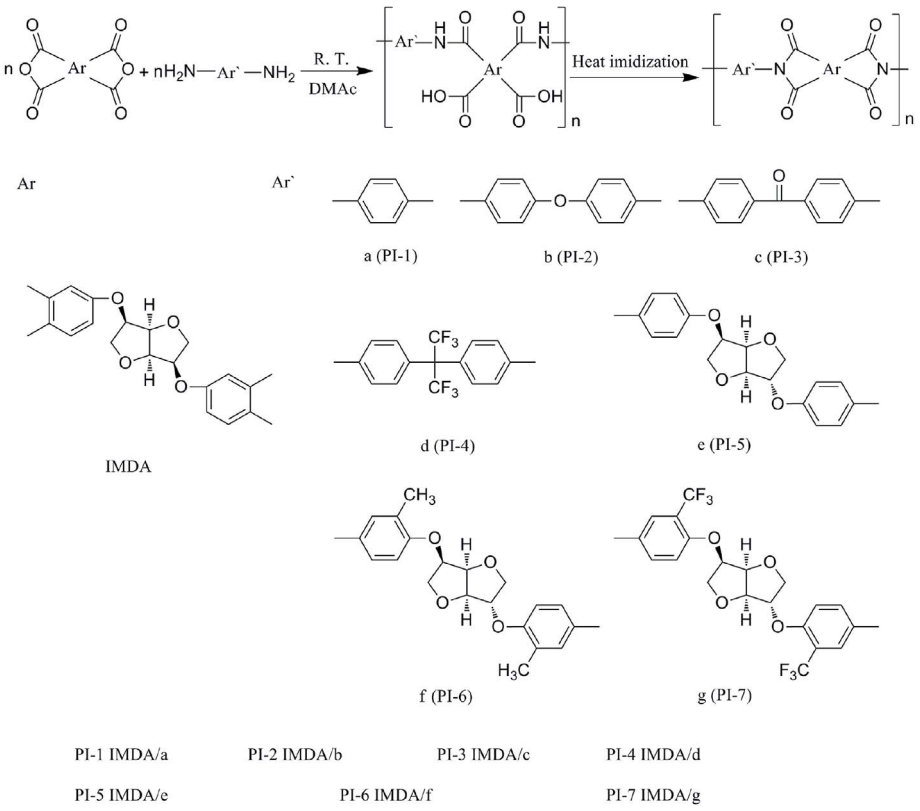

Scheme 2. Preparative route of polyimides.

graphite-monochromated Cu Kα radiation (λ = 1.5406 Å) and a 0.5 mm collimator with generator voltage and tube current at 40 KV and 40 mA, respectively. The diffraction patterns were collected at 25 °C in the reflection mode over 2 θ ranging from 5° to 50°. The transmittance of the films was determined on a Shimadzu UV–vis 2501 at 25 °C. Water uptake of polyimide films was measured by the weight changes before and after immersion in deionized water at 25 °C for 24 h, using the following equation:

$$Water\ uptake = \frac{W_{wet} - W_{dry}}{W_{dry}} \times 100\%$$

Where W_{wet} was the wet weight of the polyimide film; W_{dry} was the dry weight of the polyimide film dried in vacuo at 80 °C for 24 h with a constant weight (± 0.0001 g). Each sample was measured for five times. The dielectric constants of polyimide films were tested using an Hewlett-Packard 4285A apparatus with frequency ranging from 100 Hz to 1 MHz at 25 °C. The silver adhesive was coated into a diameter of 6 mm on both sides of the film, and measurements were conducted after the adhesive fully cured.

The geometry optimizations for the ground state (S_0) of monomers were performed using density functional theory (DFT) with the B3LYP hybrid functional and 6-31G (d, p) basis set on Gaussian 09 (version D.01) [21].

2.3. Synthesis of the monomers

2.3.1. Synthesis of 2,5-bis(3,4-dicyanophenoxy)-1,4:3,6-dianhydromannitol (IMCN)

4-Nitrophthalonitrile (5.2426 g, 0.0303 mmol) was firstly dissolved into DMAc (15 mL) to form a bright yellow homogeneous solution prior to use. Afterwards, isomannide (2.1909 g, 0.0150 mol), 60 wt% sodium hydride (1.2000 g, 0.0300 mol) and DMAc (20 mL) were fully mixed and transferred to a 100 mL ice bathed three-necked flask equipped with a magnetic stirrer, a dropping funnel, a reflux condenser, and a nitrogen inlet. Subsequently, the 4-nitrophthalonitrile solution was cautiously added dropwise to maintain the temperature of the mixture at 0 °C. After approximately 1 h, a heterogeneous black mixture was obtained and kept stirring to room temperature. The reaction progress was monitored by TLC on silica gel plates GF254. When the reaction was over, the mixture was slowly poured into a rapidly stirred 250 mL 0.1 mol/L hydrochloric acid solution to produce yellow flocculent precipitate. The residue was recrystallized in acetonitrile to obtain a shallow yellow powder. Yield: 98%. M. p. 221–222 °C (derived from DSC). ^{1}H NMR (300 MHz, dmso-d_6) δ 8.14–7.97 (m, 2H, H^1), 7.96–7.82 (m, 2H, H^2), 7.66–7.49 (m, 2H, H^3), 5.10 (dd, J = 9.4, 4.1 Hz, 2H, H^4), 4.99 (t, J = 3.9 Hz, 2H, H^5), 3.99 (dt, J = 16.2, 8.1 Hz, 2H, H^6), 3.81 (dt, J = 16.1, 8.1 Hz, 2H, $H^{6'}$). ^{13}C NMR (75 MHz, dmso-d_6) δ 161.18 (s, C^1), 135.64 (s, C^2), 120.60 (s, C^3), 120.21 (s, C^4), 116.14 (d, J = 6.5 Hz, C^5), 115.64 (s, C^6), 106.28 (s, C^7), 80.08 (s, C^8), 77.24 (s, C^9), 70.58 (s, C^{10}). Elemental analysis: calcd for $C_{22}H_{14}N_4O_4$: C, 66.33%, H, 3.54%, N, 14.06%; Found: C, 66.29%, H, 3.53%, N, 14.04%.

2.3.2. Synthesis of 2,5-bis(3,4-dicarboxyphenoxy)-1,4:3,6-dianhydromannitol (IMCO)

A mixture of IMCN (3.9810 g, 0.0100 mol), KOH (8.9600 g, 0.1600 mol), water (40 mL) and methanol (40 mL) was stirring and heated to reflux in a 250 mL three neck flask. The solid can be dissolved in 1–2 h, and reflux was continued for 7 days till no ammonia could be detected. After filtration and removal of the residue methanol under normal pressure, the filtrate was cooled and diluted to 1 L with deionized water and acidified to pH 1–2 by 6 mol/L HCl. The precipitate was filtered off and washed thoroughly with deionized water until the filtrate became neutral. Yield: 86%. M. p. 211–212 °C (derived from DSC). ^{1}H NMR (300 MHz, dmso-d_6) δ 12.91 (s, 4H, H^1), 7.78–7.57 (m, 2H, H^2), 7.34–6.97 (m, 4H, H^{3+4}), 5.03 (dd, J = 7.7, 3.8 Hz, 2H, H^5), 4.90 (t, J = 4.3 Hz, 2H, H^6), 4.01 (dd, J = 9.2, 6.1 Hz, 2H, $H^{7+7'}$), 3.81 (dd, J = 9.1, 6.4 Hz, 2H). ^{13}C NMR (75 MHz, dmso-d_6) δ 169.04 (s, C^1), 167.33 (s, C^1), 159.95 (s, C^2), 136.91 (s, C^3), 131.12 (s, C^4), 123.13 (s,

C^5), 116.09 (s, C^6), 114.10 (s, C^7), 80.26 (s, C^8), 76.91 (s, C^9), 70.75 (s, C^{10}). HRLC–MS, *m/z*: $[M+1]^+$ calcd for $C_{22}H_{18}O_{12}$ 475.0887, found. 475.0791. Elemental analysis: calcd for $C_{22}H_{18}O_{12}$: C, 55.70%, H, 3.82%; Found: C, 55.66%, H, 3.81%.

2.3.3. Synthesis of 2,5-bis(3,4-dicarboxyphenoxy)-1,4:3,6-dianhydromannitol dianhydride (IMDA)

IMCO (3.7926 g, 0.0080 mol) was suspended in 25 mL of acetic anhydride and 25 mL of glacial acetic. The mixture was refluxed for 5 h and then hot filtered to remove any impurities, and the filtrate was cooled to room temperature under nitrogen protection. Afterwards, 10 mL of ether was added to precipitate. The residue was filtered and washed thoroughly with ether to give off-white fine crystals. Yield: 92%. M. p. 203 °C (derived from DSC). ^{1}H NMR (300 MHz, dmso-d_6) δ 8.00 (d, J = 8.4 Hz, 2H, H^1), 7.74 (d, J = 2.2 Hz, 2H, H^2), 7.58 (dd, J = 8.5, 2.3 Hz, 2H, H^3), 5.21 (dt, J = 9.8, 2.9 Hz, 2H, H^4), 5.02 (d, J = 4.0 Hz, 2H, H^5), 3.95 (ddd, J = 40.8, 9.4, 5.8 Hz, 4H, $H^{6+6'}$). ^{13}C NMR (75 MHz, dmso-d_6) δ 164.23 (s, C^1), 163.04 (s, C^2), 162.61 (s, C^3), 133.98 (s, C^4), 127.15 (s, C^5), 123.47 (s, C^6), 123.06 (s, $C^{6'}$), 110.28 (s, C^7), 80.26 (s, C^8), 77.38 (s, C^9), 70.76 (s, $C^{10+10'}$). Elemental analysis: calcd for $C_{23}H_{16}O_9$: C, 63.31%, H, 3.70%; Found: C, 63.30%, H, 3.69%.

2.4. Synthesis of the polyimide films

As described in Scheme 2, all the polyimide films were obtained *via* a conventional two-step method as previously reported [19]. Typically, for PI−1, IMDA (0.8722 g, 0.002 mol), *p*-phenylenediamine (0.2161 g, 0.0020 mol) were transferred to a 50 mL three neck flask equipped with a mechanical stir under nitrogen protection, a calcd amount of DMAc was added to make the solids content at 15%. The resulting mixture was continuously stirred for 18 h at room temperature to obtain viscous PAA solution, followed by the heat imidization of PAA solution cast onto a flat glass plate under a gradient heating temperature (80 °C for 1 h, 180 °C for 1 h, 250 °C for 1 h, 300 °C for 1 h) in the vacuum tube furnace. No control over the cooling process was carried out after the heating process. A free-standing film peeled off from the glass plate after being immersed in deionized water and was dried at 80 °C in vacuo for 24 h.

Similarly, PI−2 (IMDA/b), PI−3 (IMDA/c), PI−4 (IMDA/d), PI−5 (IMDA/e), PI−6 (IMDA/f), PI−7 (IMDA/g) were obtained by the method mentioned above.

3. Results and discussion

3.1. Monomers synthesis and characterization

As pointed out by Fenouillot [12], due to the intramolecular hydrogen bonds and steric hindrance (Fig. S1), isomannide had low reactivity and related reports were rarely found. Whereas based on the fundamental studies of Williames [22], nucleophilic substitution reaction of 4-nitrophthalimide and phenol (alcohol) derivatives can be moderately conducted. Thus, IMCN (Scheme 1) was facially synthesized under the catalysis of sodium hydride with satisfactory yield, and IMCO and IMDA were readily prepared by the reported method [23]. It was noteworthy in the third step that, unlike other wholly aromatic anhydrides [23,24], an extra reagent (e.g. ether) was needed to add into the mixture of acetic acid and acetic anhydride to precipitate IMDA, illustrating that the introduction of the aliphatic fragment resulted in a better solubility of IMDA.

Characterizations including FTIR, HRLC-MS, ^{1}H NMR, ^{13}C NMR, 2D NMR and elemental analysis were used to confirm the chemical structure of the synthetic monomers (IMCN, IMCO and IMDA). In Fig. 1, characteristic absorption peaks at 2975 and 2850 cm^{-1} (asymmetric and symmetric stretching of C-H in -CH_2) indicated that isomannide fragment was successfully embedded in the monomer. Additionally, the disappearance of the characteristic vibration of -CN around 2232 cm^{-1}

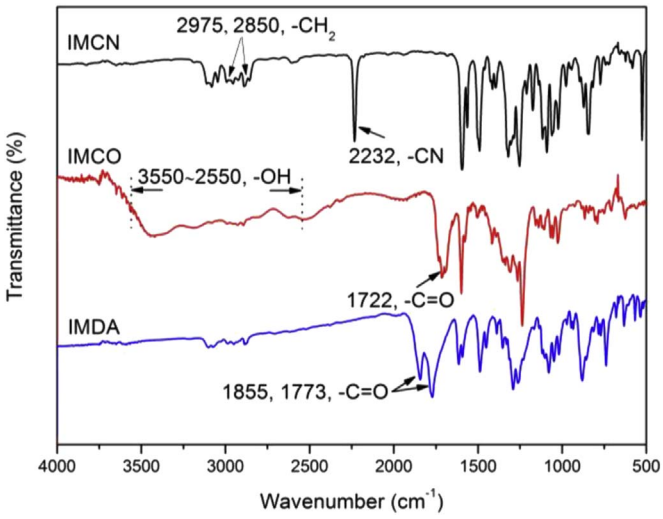

Fig. 1. FTIR spectra of IMCN, IMCO and IMDA.

and the appearance of characteristic absorption peaks near 3550 − 2550 cm^{-1} (-OH in -COOH) and 1722 cm^{-1} (-C=O in -COOH) illustrated the complete hydrolysis of IMCN. Similarly, the disappearance of the hydroxyl absorption peaks at 3550 − 2550 cm^{-1} and the appearance of characteristic absorption peaks near 1855 cm^{-1}, 1773 cm^{-1} (asymmetric and symmetric stretching of -C=O) proved the thorough dehydration and cyclization of carboxyl in IMCO. Moreover, compared with the ^{1}H NMR spectrum of IMCN in Fig. 2A, the appearance of the proton (-COOH of IMCO) resonance at 12.91 ppm in Fig. 2C also demonstrated the hydrolysis of IMCN, which was consistent with the FTIR results. Meanwhile, ^{13}C NMR spectra of IMCN and IMCO shown in Fig. 2B and D also presented unambiguously assignment of each carbon atom. Further, ^{1}H and ^{13}C NMR spectra of IMDA were presented in Fig. 3A and Fig. 3C, respectively, and 500 MHz ^{1}H–^{1}H COSY and ^{1}H–^{13}C HSQC spectra shown in Fig. 3B and D were respectively utilized to fully accomplish the proton and carbon peak assignment of IMDA. As displayed in Fig. 3B, the cross-peaks H^1/H^3, H^4/H^5, H^4/H^6 and $H^4/H^{6'}$ found in the COSY spectrum at 8.00/7.58, 5.21/5.02, 5.21/4.01 and 5.21/3.90 ppm illustrated the existence of H^1, H^3, H^4, H^5, H^6 and $H^{6'}$, respectively. In addition, corresponding carbon atoms linked to hydrogen atoms were also found by HSQC spectrum. As exhibited in Fig. 3D, the HSQC signals at 8.00/127.15, 7.74/110.28 and 7.58/123.47 ppm were ascribed to H^1/C^5, H^2/C^7 and H^3/C^6, while H^4/C^9, H^5/C^8, H^6/C^{10} and $H^{6'}/C^{10'}$ signals were found at 5.21/77.38, 5.02/80.26, 4.01/70.76 and 3.90/70.76 ppm, respectively.

3.2. Polyimides synthesis

As described in Scheme 2, all the polyimides were prepared *via* soluble poly(amic acid) (PAA) precursors, followed by heat imidization at a gradient temperature, Characterizations including FTIR spectra, ^{1}H NMR spectra and elemental analysis were used to confirm the chemical structure of polyimides.

As depicted in Table S1, the viscosity of polyamic acid solution exhibited a range of 0.98–1.62 dL/g at 25 °C, and M_w and polydispersities (M_w/M_n) of corresponding polyimides covered a range of 60,249 − 90,876 and 1.20–1.54, respectively, illustrating the relatively high molecular weights. Moreover, FTIR spectra of all the polyimides were presented in Fig. 4, characteristic absorptions peaks around 2975 and 2884 cm^{-1} (asymmetric and symmetric stretching of C-H in -CH_2) and 1100 cm^{-1} (asymmetric stretching of alicyclic C-O-C) indicated the existence of 1,4:3,6-dianhydrohexitol residues. The appearance of peaks near 1781 cm^{-1} (asymmetrical stretching of C=O), 1722 cm^{-1} (symmetrical stretching of C=O) and 1379 cm^{-1} (C-N stretching) and

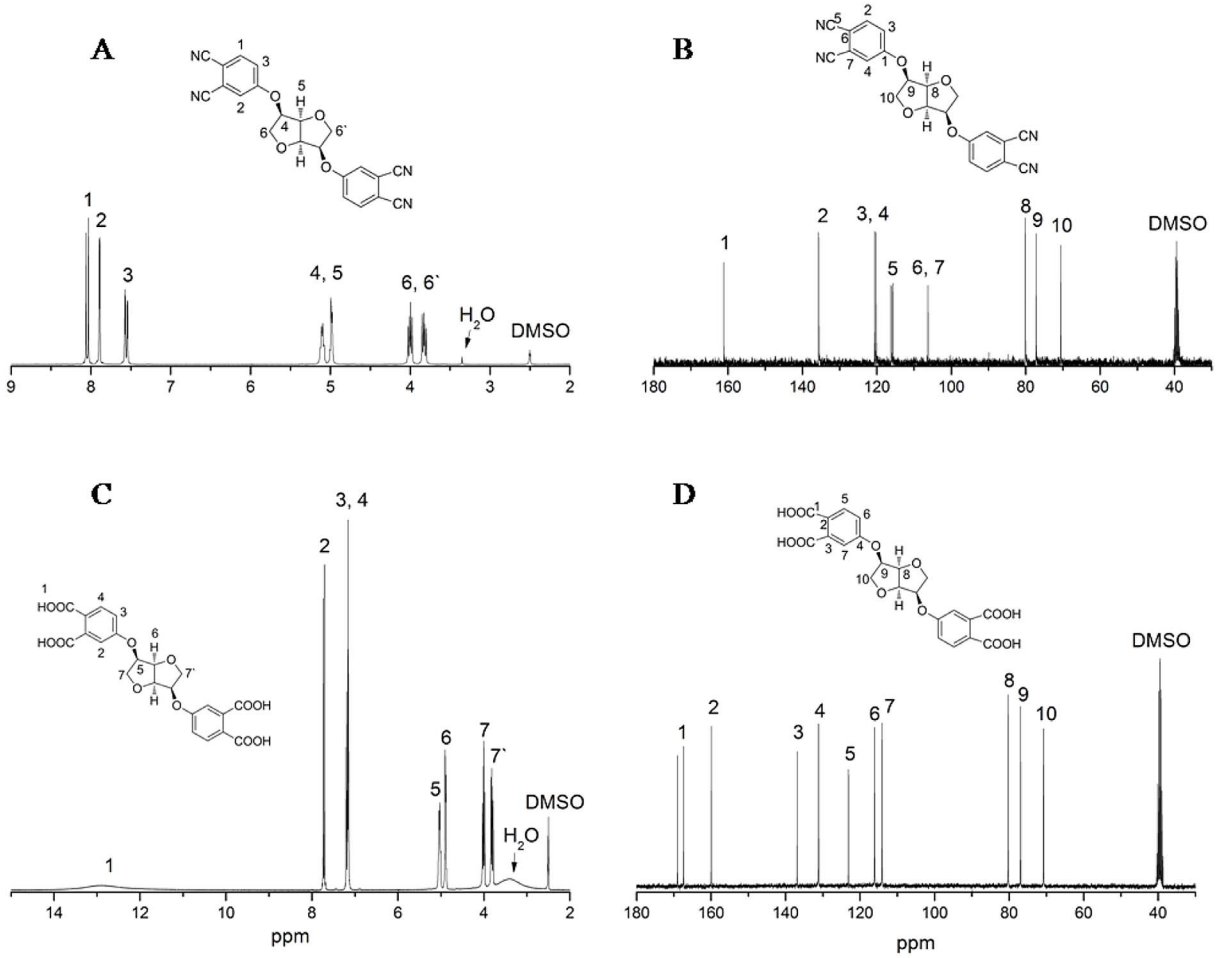

Fig. 2. (A) ^{1}H NMR spectrum of IMCN; (B) ^{13}C NMR spectrum of IMCN; (C) ^{1}H NMR spectrum of IMCO; (D) ^{13}C NMR spectrum of IMCO.

the disappearance of peaks around 3220 − 3450 cm^{-1} (N-H stretching) and 1580 − 1620 cm^{-1} (N-H bend) could elucidate the thorough imidization of polyamic acid. Furthermore, ^{1}H NMR spectra of PI − 6 were described as a typical representative shown in Figs. 1, 4 and 5:3,6-dianhydrohexitol fragments displayed resonances at δ 3.90–5.22 ppm and the protons of -CH_3 exhibited resonances at δ 2.17–2.23 ppm, which confirmed the successful integration of alicyclic segments into the polyimide skeleton.

3.3. Thermal properties

To fully evaluate the thermal properties of PI − (1–7), measurements including DSC, DMA, TMA and TGA were conducted and the results were listed in Table 1. As displayed in Fig. 6, the synthetic polyimides exhibited T_g of 214–300 °C by DSC and 229–281 °C by DMA, respectively, which indicated their good thermal property and can be comparable with other reported polyimides containing alicyclic fragments [24]. Classically, according to the Kuhn and Flory theories [19,25] in regard with conformational rigidity of polymers, the conformational rigidity of a single chain could be reasonably assumed to be dictated by the rigidity of the repeating units. For PI − (1–4), PI − 1 (IMDA/a, 300 °C) displayed the highest T_g, which could be ascribed to the rigid *p*-phenylenediamine residues in the molecular chains. Whereas the relatively low T_g of PI − 2 (IMDA/b, 250 °C) might have a close relationship with the flexible rotary ether bond derived from 4,4′-ODA segment. A higher T_g of PI − 4 (IMDA/d, 277 °C) than that of PI − 3 (IMDA/c, 267 °C) was probably attributed to the larger steric limitations endowed by the sp^3-swivel moiety of hexafluoroisopropyl [26]. Interestingly, PI − 4 exhibited 17 °C higher of T_g than that of our previous reported analogue ref.PI − 7 (2c/6FDA, 260 °C) [19], which might be ascribed that the exo-exo oriented 'boat' structure of isomannide residue in PI − 4 owned a stiffer conformation than that of the endo-exo oriented 'chair' structure of isosorbide residue in ref.PI − 7, which can be evidenced by geometric optimization of two segments by Gaussian 09 computation (Fig. S2). Additionally, an extra melting point for PI − 5 (IMDA/e, 214 °C) was observed at 339 °C, illustrating that PI − 5 possessed a semicrystalline morphology. The T_g of PI − 5 (IMDA/e, 214 °C) and PI − 6 (IMDA/f, 218 °C) was 19 °C and 15 °C lower than that of PI − 7 (IMDA/g, 233 °C), respectively, which may be attributed that steric hindrance of bulky trifluoromethyl made the molecular chains difficult to move. Simultaneously, DMA curves shown in Fig. 6B exhibited slight difference of T_g with that of DSC results, which was due to the distinguished responses of the samples to the two characterization methods. Notablely, for PI − 1, neither apparent T_g nor significant drop of the storage modulus was observed even at 350 °C, which might further elucidate its rigid polymer chains.

As demonstrated in Fig. S3, PI − (1–7) presented relatively low CTE values (25 ppm K^{-1} − 55 ppm K^{-1}) and can be comparable to some aromatic polyimides (47.4–63.2 ppm K^{-1}) [27], implying their good dimensional stability. Popularly, the rigidity and linearity of polymer chains were the dominant factor affecting the CTE values, as listed in Table 1, PI − (5–7) exhibited the higher CTE values than that of PI − (1–4), which can be explained by the larger amounts of distorted and flexible structure of 1,4:3,6-dianhydrohexitol residues. The lowest CTE value of PI − 1 (25 ppm K^{-1}) could be attributed to the rigid linear polymer chains whereas relatively twisted and flexible structure endowed PI − 6 a higher CTE (55 ppm K^{-1}) value than that of the other polyimides. Distinctively, PI − 1 and PI − 3 exhibited negative CTE

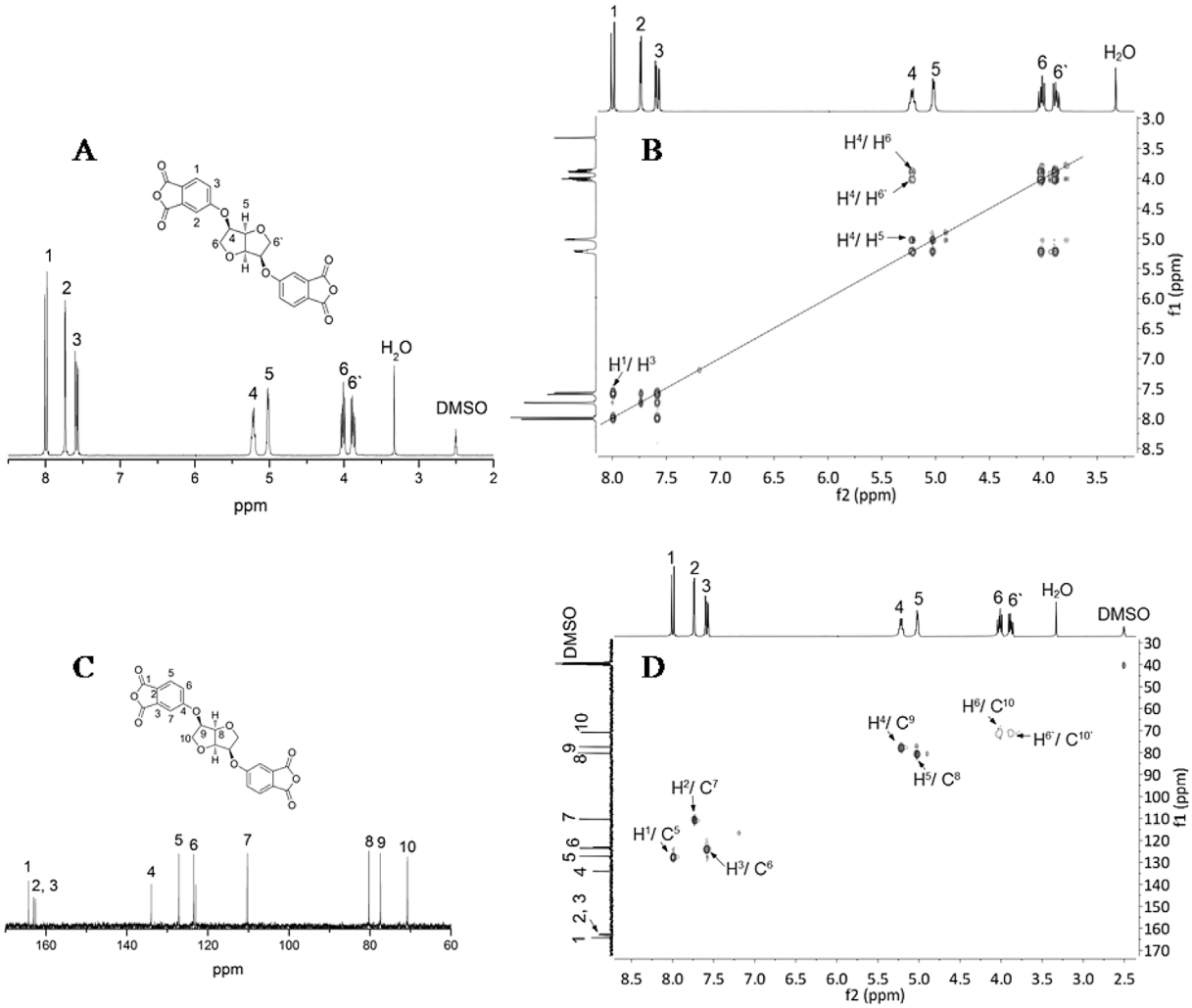

Fig. 3. (A) ^{1}H NMR spectrum of IMDA; (B) 500 MHz correlation spectrum (COSY) of IMDA; (C) ^{13}C NMR spectrum of IMDA; (D) 500 MHz heteronuclear single quantum correlation (HSQC) spectrum of IMDA.

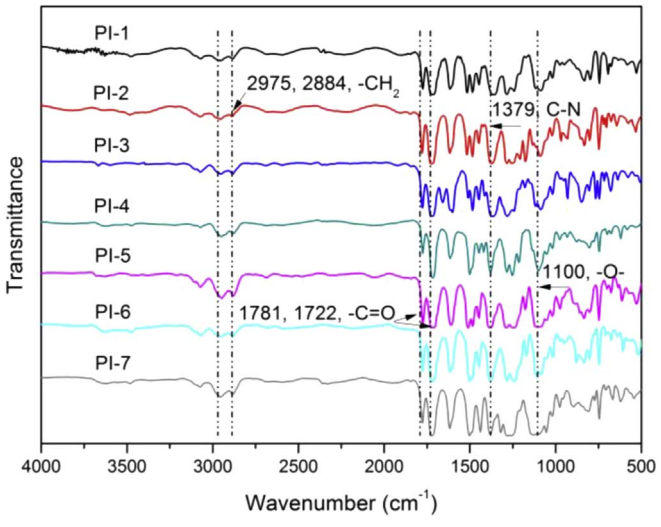

Fig. 4. FTIR spectra of polyimides.

values (insert picture in Fig. S3) at the higher temperature, which might be due to their high extents of in-plane orientation [28,29].

TGA curves of polyimide films both in N_2 and in air were described in Fig. 7 and the results were summarized in Table 1. No obvious thermal decomposition could be observed before 415 °C in N_2, and 5% weight loss temperature ($T_{5\%}$) in N_2 and in air were located in the range of 415–453 °C and 376–433 °C, respectively, which indicated their high thermal stability. For PI−(1–4), $T_{5\%}$ and $T_{10\%}$ in air were higher than that of PI−(5–7), which was probably ascribed that the aromatic diamine segments occupied higher thermal decomposition temperature than that of isosorbide derived ones [30]. In addition, thermal decomposition of PI−(1–7) was divided into two stages, as can be seen from the typical DTG curves of PI−3 in Fig. 7B, the first stage at 428–483 °C was corresponding to the decomposition of the aliphatic residues, which was probably caused by the oxidation at the carbon atom in the α-position of the ether oxygens in 1,4:3,6-dianhydrohexitol units [13]; while the second one at 559–658 °C was corresponding to the decomposition of the aomatic fragments [30].

3.4. Mechanical and morphological properties

Mechanical properties of polyimides were evaluated at 23 ± 2 °C and a relative humidity of 50 ± 5% based on ASTM D882-02 standard, and the results were summarized in Table 2. The polyimide films exhibited the tensile strength (T_S), tensile modulus (T_M) and elongation at break (E_B) in range of 79–153 MPa, 1.9–4.2 GPa and 6–15%, respectively. In general, the incorporation of aliphatic chains into polyimides led to a decrement of their mechanical properties [31], however, PI−(1–7) exhibited surprisingly comparable mechanical properties

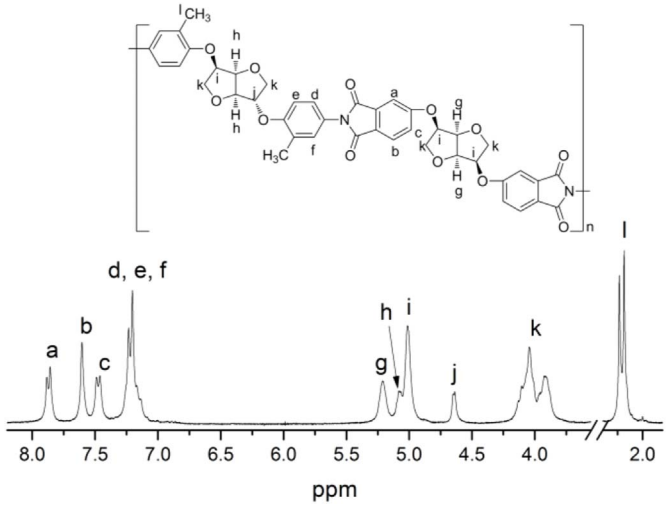

Fig. 5. ^{1}H NMR spectrum of PI–6 (IMDA/f).

Table 1
Thermal properties analyzed from DSC, DMA, TGA and TMA.

Polyimides	T_g (°C)		$T_{5\%}$ (°C)[c]		$T_{10\%}$ (°C)[c]		R_W (°C)[d]	CTE (ppm K^{-1})[e]
	DSC[a]	DMA[b]	In N_2	In air	In N_2	In air		
PI−1	300	ND[f]	447	399	458	415	45	25
PI−2	250	258	450	429	460	448	47	37
PI−3	267	256	447	433	459	448	47	35
PI−4	277	281	453	426	464	447	37	34
PI−5	214	229	432	394	440	418	29	48
PI−6	218	230	415	376	426	414	33	55
PI−7	233	237	432	387	445	406	42	51

[a] Obtained at the baseline shift in the second heating DSC traces, the temperature was raised at 10 °C/min with a nitrogen flow rate at 50 mL/min.
[b] Measured by DMA with a heating rate of 5 °C/min and a load frequency of 1 Hz in film tension geometry in air.
[c] 5% and 10% weight loss temperatures measured by TGA, the temperature was raised at 10 °C/min with a nitrogen flow rate at 50 mL/min.
[d] Residual weight retention at 800 °C by TGA, the temperature was raised at 10 °C/min with a nitrogen flow rate at 50 mL/min.
[e] CTE, coefficient of thermal expansion was recorded from 50 °C to 150 °C, the temperature was raised at 10 °C/min with a nitrogen flow rate at 80 mL/min.
[f] ND, not detected.

with that of the reported aromatic polyimides [32], implying that diamines and dianhydride (IMDA) containing 1,4:3,6-dianhydrohexitol units owned parallel stiffness and toughness with the aromatic ones. Surprisingly, PI−1 displayed the highest T_S of 153 MPa and was approximately equivalent to Kapton 100CR (PMDA/4,4′-ODA, 152 MPa, Dupont) [33], which was probably related to the relatively fixed 'boat' conformation of the isomannide residue and the nonflexible planar structure of the *p*-phenylenediamine segment, as well as the high molecular weight of the polymer. Compared with PI−1, moderate T_S (103–118 MPa) of PI−2 and PI−(5–7) might be attributed to their relatively bent and distorted structure, resulting in the weaker interaction of molecular chains. Moreover, PI−3 owned far higher T_S (132 MPa) than that of PI−4 (79 MPa) despite their similar low molecular weights, which may be a result of the crosslinking of benzophenone C=O groups during thermal imidization process [34].

Wide-angle X-ray Diffraction was used to analyze the morphological structure of the polyimide films. As described in Fig. 8, one halo was observed with 2 θ varying 13–22° and the calcd d-space of molecular chains was 0.497–0.560 nm. The semicrystalline morphology of polyimides such as PI−1 and PI−5 illuminated that 1,4:3,6-dianhydrohexitols possessed a certain degree of regularity. Unlike PI−5, no melting peak appeared for PI−1 in DSC trace, which was probably ascribed that the melting point was too high to be detected [35]. Moreover, the amorphous morphology of PI−6 and PI−7 in comparison with PI−5 might be a result of the incorporation of methyl and bulk pendent trifluoromethyl, leading to the looser stacking of molecular chains, which can be verified by comparing d-space shown in Table 2, PI−5 (0.497 nm) < PI−6 (0.548 nm) < PI−7 (0.552 nm) [36]. Other polyimides like PI−2, PI−3 and PI−4 were amorphous, which can be explained that their flexible ether linkages or pendent groups loosened the chain packing of the polymers.

3.5. Solubility

Solubility test was carried out at 25 °C by dissolving 10 mg of polyimide in 1 mL of solvent for 24 h and the results were summarized in Table 3. It can be found that almost all the polyimides possessed superior solubility in common polar solvents like *N,N*-dimethylformamide (DMF), *N,N*-dimethylacetamide (DMAc) and *N*-methyl-2-pyrrolidone (NMP). Compared with PI−(1–4), PI−(5–7) owned the better solubility, which might be related to the presence of more cycloaliphatic 1,4:3,6-dianhydrohexitol units: the wedge-shaped structure of two five-membered rings (dihedral angle ≈ 120°) loosened molecular chain packing and weakened the intermolecular interaction. The solubility of PI−(1–4) showed an order of PI−4 > PI−2 > PI−1 > PI−3, the inferior solubility of PI−3 might be a result of the

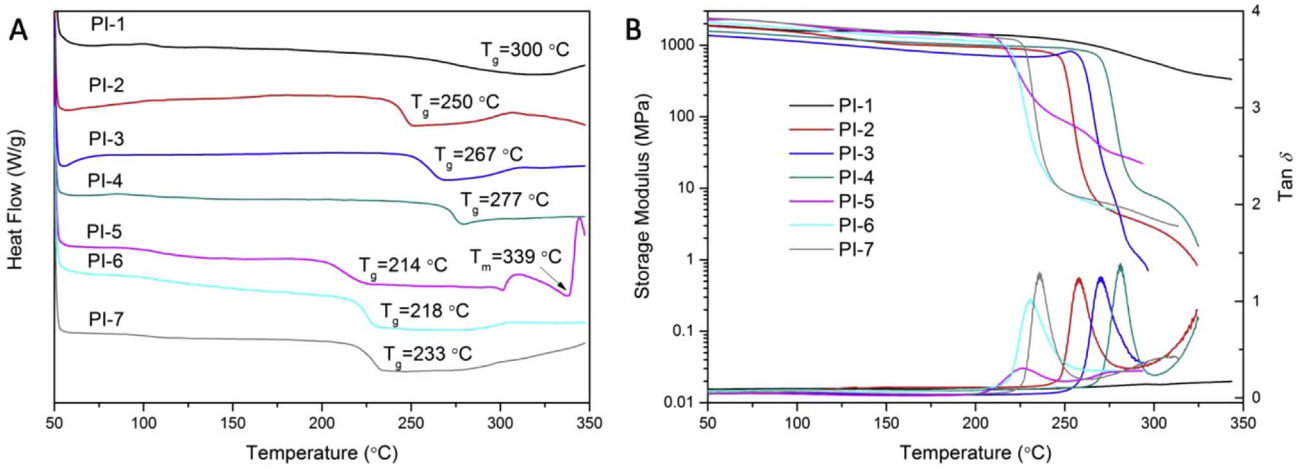

Fig. 6. (A) DSC traces of polyimide films; (B) Storage modulus and tan δ curves of polyimide films measured by DMA.

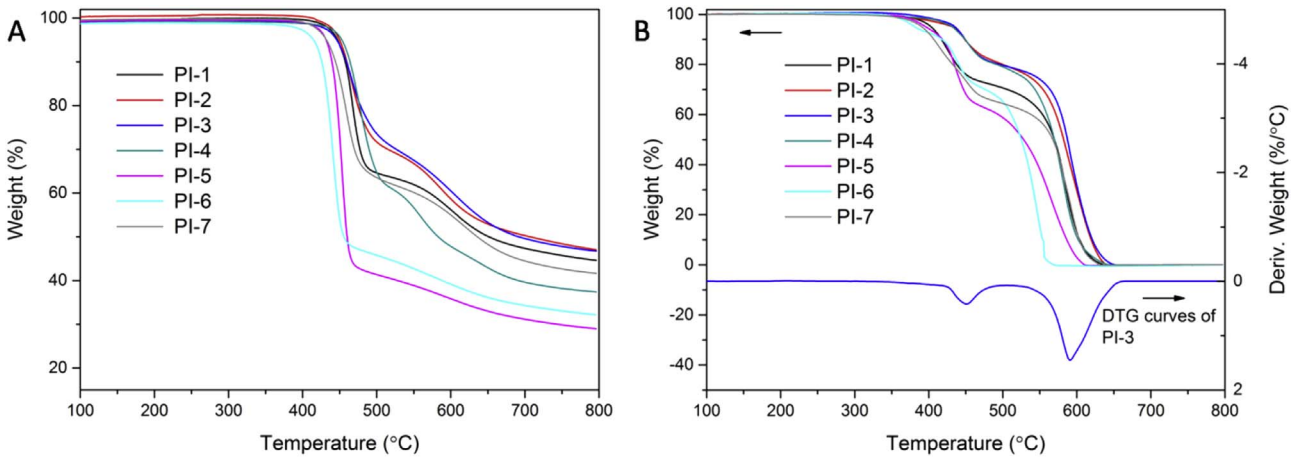

Fig. 7. (A) TGA curves of PI−(1–7) in N_2; (B) TGA and DTG curves of PI−(1–7) and DTG curves of PI−3 in air.

Table 2
Mechanical properties and X-ray diffraction spacings of polyimides.

Polyimides	T_S[a] (MPa)	T_M[b] (GPa)	E_B[c] (%)	2 θ (deg)	X-ray diffraction (nm)[d]
PI−1	153 ± 3.9[e]	4.2 ± 0.10	14 ± 0.3	17.115	0.518
PI−2	115 ± 1.6	2.8 ± 0.06	13 ± 0.1	16.793	0.528
PI−3	132 ± 1.6	3.3 ± 0.11	11 ± 0.9	16.138	0.549
PI−4	79 ± 0.7	2.6 ± 0.04	6 ± 0.1	15.813	0.560
PI−5	108 ± 1.1	1.9 ± 0.02	12 ± 0.3	17.851	0.497
PI−6	118 ± 2.1	2.9 ± 0.10	10 ± 0.2	16.161	0.548
PI−7	103 ± 1.8	2.1 ± 0.04	15 ± 0.4	16.057	0.552

[a] T_S, Tensile strength.
[b] T_M, Tensile modulus.
[c] E_B, Elongation at break.
[d] X-ray diffraction: the average distance between the molecular chains (d-space) was calculated by the Bragg equation $\lambda = 2d \sin\theta$ (λ = 1.5406 Å).
[e] 3.9, standard deviation.

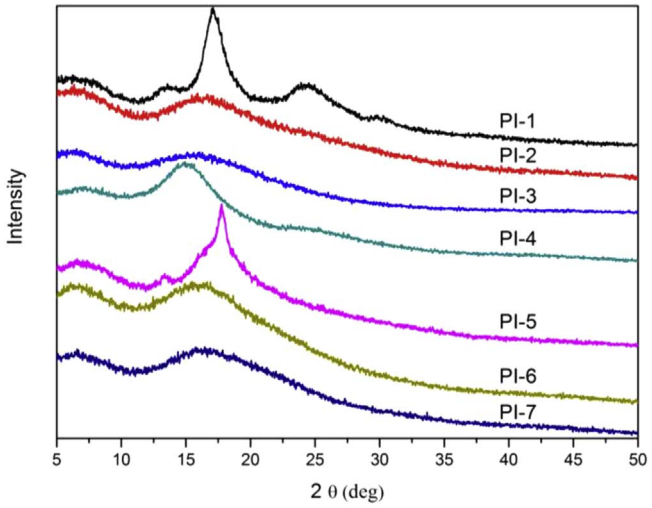

Fig. 8. X-ray film diffraction patterns of polyimides at 25 °C.

crosslinking of benzophenone C=O groups during thermal imidization process, while the existence of bent and bulky hexafluoroisopropyl endowed PI−4 better soluble performance. Interestingly, non-fluorinated PI−5 demonstrated similar solubility to that of fluorinated ref.PI−7 [19], which was inconsistent with our former finding that alicyclic isosorbide residue was inferior in enhancing the solubility of polymers than that of trifluoromethyl [19], illustrating that 1,4:3,6-dianhydrohexitol in dianhydride was more influential than that in diamine on the determination of polymers solubility. The better solubility of PI−6 and PI−7 than that of PI−5 may be attributed to the fact that the integration of methyl and trifluoromethyl made the molecular chains pack looser. It was worth noting that the ease of processability using common organic solvents, especially low boiling solvents, made these polymers suitable for solution processing techniques.

Table 3
Solubility properties of the polyimide films.

Solvents	PI−1	PI−2	PI−3	PI−4	PI−5	PI−6	PI−7
DMAc[a]	++	++	++	++	++	++	++
DMF	++	++	++	++	++	++	++
NMP	+−	++	++	++	++	++	++
DMSO	+−	+−	−	++	+−	++	++
THF	+−	+−	+−	++	++	++	++
m-Cresol	+−	+−	+−	+−	+−	+−	++
$CHCl_3$	−	−	−	+−	+−	+−	+−
1,4-dioxane	−	−	−	+−	−	+−	+−

[a] DMAc = *N,N*-dimethylacetamide; DMF = *N,N*-dimethylformamide; THF = Tetrahydrofuran. NMP = *N*-methyl-2-pyrrolidone; DMSO = Dimethyl sulfoxide; ++, soluble at 25 °C; +−, partial soluble; −, insoluble.

3.6. Optical properties

UV–vis spectroscopy was utilized to characterize the optical transparency of polyimide films with thickness at approximately 20 μm. As displayed in Fig. 9, almost all the polyimides possessed outstanding transmittance (> 80%) at 450 nm, except for PI−3, lower than 73%, which might be due to the crosslinking of benzophenone C=O groups which was conducive to CT interaction. Existence of twisted linkages and bulky hexafluoroisopropyl in PI−2 and PI−4 might render their higher transmittance than that of PI−1. Notably, the transmittance of PI−5 and ref.PI−7 [19] exhibited a similar situation with their solubility, implying that polyimides simultaneously containing 1,4:3,6-dianhydrohexitol units in diamine and dianhydride exhibited comparable optical performance with the alicyclic fluorinated ones, and 1,4:3,6-dianhydrohexitol fragment in dianhydride was more determinant in transmittance of polyimides than that in diamine. Generally, the incorporation of side groups (methyl or trifluoromethyl) can significantly loosen the molecular chain packing and thus result in the weakened CT interaction and the improved transparency [37]. Unexpectedly, compared with PI−5 (86%), the transmittance of PI−7 was increased by only 3%. Explanation can be sought from the original discrepant effects of alicyclic segments and substituents (e.g. trifluoromethyl) on CT interaction: the aliphatic residues possessed weak

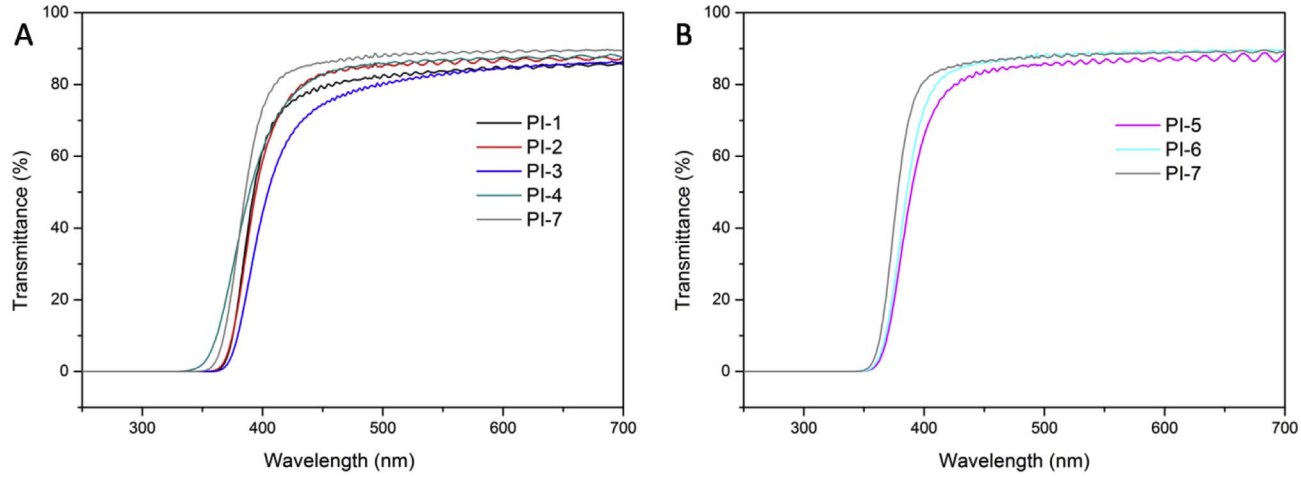

Fig. 9. (A) UV–vis curves of PI−(1–4) and PI−7; (B) UV–vis curves of PI−(5–7) with thickness at 20 μm.

electro-donatability and thus can significantly reduce the intra- and intermolecular conjugation [18], whereas the presence of trifluoromethyl mainly increase the steric hindrance which could result in the looser molecular chains [38]. Therefore, it can be speculated that the incorporation of 1,4:3,6-dianhydrohexitol fagments can reduce the CT interaction not only by hindering intra- and intermolecular conjugation, but also by the looser molecular chains caused by wedge-shaped structure of 1,4:3,6-dianhydrohexitol fagments. For PI−5, the presence of the wedge-shaped alicyclic structure both in dianhydride and diamine resiudes possibly led to an 'already' weakened CT interaction regardless of the introduction of the methyl (in PI−6) or trifluoromethyl (in PI−7). The slight improvement of transmittance for 3% might be a result of low polarizability of the C-F linkage which induced a weaker intermoleculer cohensive force and hence the subdued CT interaction [39].

3.7. Biobased content, water uptakes and dielectric constants

According to ASTM D 6866–05, biobased content of a product was defined as the "amount of biobased carbon in the material or product as a percent of the weight (mass) of the total organic carbon in the product" [40]. As a result, biobased content (Table 4) of PI−(1–7) can be calculated at 17.1%–30.0%, which met or were close to the US Department of Agriculture (USDA) minimum requirement for bio-based products (25%) [18].

Water uptakes and dielectric constants (shown in Fig. S4) of polyimides were also assessed and the results were listed in Table 4. Water uptakes and dielectric constants displayed a range of 0.25–0.39% and 2.14–2.94 (100 Hz–1 MHz), which were distinctly lower than that of the reported ones [32]. PI−5 containing isosorbide unit in diamine fragment exhibited lower dielectric constant than that of PI−2, and so was the case for PI−7 and PI−4, which might be attributed that alicyclic segments in polyimides could lead to lower hydrophobicity and polarity [41]. Inconsistent with the optical properties behavior, PI−7 (2.14 at 1 MHz) showed obviously lower dielectric constants than that of PI−5 (2.82 at 1 MHz), which had a greater relationship with the large free volume, strong electronegativity and low polarizability of trifluoromethyl.

4. Conclusions

In this study, a novel dianhydride containing 1,4:3,6-dianhydro-D-mannitol unit, IMDA was successfully prepared and polycondensed with aromatic and semiaromatic diamines to obtain two series of polyimides *via* a two-step thermal imidization, and their structure-property relationships were discussed in detail. All the polyimides possessed excellent solubility in polar solvents and outstanding transmittance as high as 89% at 450 nm. Compared with PI−(1–4), PI−(5–7) owned the better solubility and the higher transmittance, which was mainly attributed to the presence of more cycloaliphatic 1,4:3,6-dianhydrohexitol units: the wedge-shaped structure of two five-membered rings loosened molecular chain packing and weakened the intermolecular interaction, and their weak electro-donatability can significantly reduce the intra- and intermolecular conjugation; simultaneously, it was concluded that 1,4:3,6-dianhydrohexitol fragment in dianhydride was more determinant in solubility and transmittance of polyimides than that in diamine. Additionally, all the polyimides exhibited satisfactory thermal and mechanical properties, especially for

Table 4
Biobased content, optical, water uptakes and dielectric constants of polyimide films.

[a] Polyimides Film	[b] Biobased content (%)	[c] Transmittance (%)	[d] $\lambda_{cut\text{-}off}$ (nm)	Water uptakes (%)	Dielectric constants			
					1 KHz	10 KHz	100 KHz	1 MHz
PI−1	21.4	80	351	0.36	2.90	2.86	2.80	2.69
PI−2	17.6	82	347	0.33	2.85	2.82	2.76	2.67
PI−3	17.1	73	353	0.39	2.94	2.91	2.89	2.82
PI−4	16.2	83	325	0.27	2.63	2.54	2.43	2.26
PI−5	30.0	86	340	0.30	2.76	2.74	2.70	2.62
PI−6	28.5	88	339	0.31	2.69	2.66	2.62	2.53
PI−7	28.5	89	333	0.25	2.52	2.43	2.31	2.14

[a] Film thickness at 20 μm.
[b] Biobased content was calculated based on ASTM D 6866–05.
[c] Transmittance at 450 nm.
[d] Cut-off wavelength.

PI−1, its T_S was 153 MPa and approximately equivalent to that of Kapton 100CR (152 MPa), which had a close relationship with the relatively fixed 'boat' conformation of 1,4:3,6-dianhydrohexitol fragments as well as their high molecular weights. Furthermore, these polymers also exhibited low dielectric constants as well as water uptakes, which may be connected with the hydrophobic effect and low polarity of the 1,4:3,6-dianhydrohexitol segments. Their satisfactory overall performance, particularly, excellent transmittance and processability combined with dimensional stability and mechanical properties made these polymers ideal candidates for optoelectronic device substrates.

Acknowledgments

We were grateful to Teacher Chunyu Wang for 2D NMR test and Dr. Changjiang Zhou for molecular geometry optimizations.

Appendix A. Supplementary data

Supplementary data related to this article can be found at http://dx.doi.org/10.1016/j.polymdegradstab.2018.01.006.

References

[1] J.A. Spechler, T.-W. Koh, J.T. Herb, B.P. Rand, C.B. Arnold, A transparent, smooth, thermally robust, conductive polyimide for flexible electronics, Adv. Funct. Mater. 25 (2015) 7428–7434.
[2] D.S. Ghosh, T.L. Chen, V. Mkhitaryan, V. Pruneri, Ultrathin transparent conductive polyimide foil embedding silver nanowires, ACS Appl. Mater. Interfaces 6 (2014) 20943–20948.
[3] D.P. Erhard, F. Richter, C.B.A. Bartz, H.-W. Schmidt, Fluorinated aromatic polyimides as high-performance electret materials, Macromol. Rapid Commun. 36 (2015) 520–527.
[4] W. Chen, Z. Zhou, T. Yang, R. Bei, Y. Zhang, S. Liu, Z. Chi, X. Chen, J. Xu, Synthesis and properties of highly organosoluble and low dielectric constant polyimides containing non-polar bulky triphenyl methane moiety, React. Funct. Polym. 108 (2016) 71–77.
[5] K.-H. Nam, H. Kim, H.K. Choi, H. Yeo, M. Goh, J. Yu, J.R. Hahn, H. Han, B.-C. Ku, N.-H. You, Thermomechanical and optical properties of molecularly controlled polyimides derived from ester derivatives, Polymer 108 (2017) 502–512.
[6] H. Yeo, M. Goh, B.-C. Ku, N.-H. You, Synthesis and characterization of highly-fluorinated colorless polyimides derived from 4,4′-((perfluoro-[1,1′-biphenyl]-4,4′-diyl)bis(oxy))bis(2,6-dimethylaniline) and aromatic dianhydrides, Polymer 76 (2015) 280–286.
[7] I.S. Chung, C.E. Park, M. Ree, S.Y. Kim, Soluble polyimides containing benzimidazole rings for interlevel dielectrics, Chem. Mater. 13 (2001) 2801–2806.
[8] S.D. Kim, S.Y. Kim, I.S. Chung, Soluble and transparent polyimides from unsymmetrical diamine containing two trifluoromethyl groups, J. Polym. Sci., Part A: Polym. Chem. 51 (2013) 4413–4422.
[9] L. Yi, W. Huang, D. Yan, Polyimides with side groups: synthesis and effects of side groups on their properties, J. Polym. Sci., Part A: Polym. Chem. 55 (2017) 533–559.
[10] H.-J. Ni, J.-G. Liu, Z.-H. Wang, S.-Y. Yang, A review on colorless and optically transparent polyimide films: chemistry, process and engineering applications, J. Ind. Eng. Chem. 28 (2015) 16–27.
[11] H.-Y. Lu, C.-Y. Chou, J.-H. Wu, J.-J. Lin, G.-S. Liou, Highly transparent and flexible polyimide-AgNW hybrid electrodes with excellent thermal stability for electrochromic applications and defogging devices, J. Mater. Chem. C 3 (2015) 3629–3635.
[12] F. Fenouillot, A. Rousseau, G. Colomines, R. Saint-Loup, J.P. Pascault, Polymers from renewable 1,4:3,6-dianhydrohexitols (isosorbide, isomannide and isoidide): a review, Prog. Polym. Sci. 35 (2010) 578–622.
[13] L. Jasinska, M. Villani, J. Wu, D. van Es, E. Klop, S. Rastogi, C.E. Koning, Novel, fully biobased semicrystalline polyamides, Macromolecules 44 (2011) 3458–3466.
[14] B.A.J. Noordover, V.G. van Staalduinen, R. Duchateau, C.E. Koning, B. van, M. Mak, A. Heise, A.E. Frissen, J. van Haveren, Co- and terpolyesters based on isosorbide and succinic acid for coating applications: synthesis and characterization, Biomacromolecules 7 (2006) 3406–3416.
[15] R. Marín, A. Alla, A. Martínez de Ilarduya, S. Muñoz-Guerra, Carbohydrate-based polyurethanes: a comparative study of polymers made from isosorbide and 1,4-butanediol, J. Appl. Polym. Sci. 123 (2012) 986–994.
[16] D. Juais, A.F. Naves, C. Li, R.A. Gross, L.H. Catalani, Isosorbide polyesters from enzymatic catalysis, Macromolecules 43 (2010) 10315–10319.
[17] M. Śmiga-Matuszowicz, B. Janicki, K. Jaszcz, J. Łukaszczyk, M. Kaczmarek, M. Lesiak, A.L. Sieroń, W. Simka, M. Mierzwiński, D. Kusz, Novel bioactive polyester scaffolds prepared from unsaturated resins based on isosorbide and succinic acid, Mater. Sci. Eng. C 45 (2014) 64–71.
[18] X. Ji, Z. Wang, J. Yan, Z. Wang, Partially bio-based polyimides from isohexide-derived diamines, Polymer 74 (2015) 38–45.
[19] Z. Mi, Z. Liu, C. Tian, X. Zhao, H. Zhou, D. Wang, C. Chen, Soluble polyimides containing 1,4:3,6-dianhydro-d-glucidol and fluorinated units: preparation, characterization, optical, and dielectric properties, J. Polym. Sci., Part A: Polym. Chem. 55 (2017) 3253–3265.
[20] X. Ji, J. Yan, X. Liu, Z. Wang, Z. Wang, Synthesis and properties of polyimides derived from bis(4-aminophenyl)isohexides, High Perform. Polym. 29 (2016) 197–204.
[21] Y. Gao, S. Zhang, Y. Pan, L. Yao, H. Liu, Y. Guo, Q. Gu, B. Yang, Y. Ma, Hybridization and de-hybridization between the locally-excited (LE) state and the charge-transfer (CT) state: a combined experimental and theoretical study, Phys. Chem. Chem. Phys. 18 (2016) 24176–24184.
[22] F.J. Williams, P.E. Donahue, Reactions of phenoxides with nitro- and halo-substituted phthalimides, J. Org. Chem. 42 (1977) 3414–3419.
[23] X. Ma, B. Ghanem, O. Salines, E. Litwiller, I. Pinnau, Synthesis and effect of physical aging on gas transport properties of a microporous polyimide derived from a novel spirobifluorene-based dianhydride, ACS Macro Lett. 4 (2015) 231–235.
[24] H. Zhao, G. Chen, Y. Zhou, X. Li, X. Fang, Synthesis and characterization of organosoluble and transparent polyimides derived from trans-1,2-bis(3,4-dicarboxyphenoxy)cyclohexane dianhydride, J. Appl. Polym. Sci. 132 (2015) 42317.
[25] B. Erman, P.J. Flory, J.P. Hummel, Moments of the end-to-end vectors for p-phenylene polyamides and polyesters, Macromolecules 13 (1980) 484–491.
[26] D.H. Wang, J.J. Wie, K.M. Lee, T.J. White, L.-S. Tan, Impact of backbone rigidity on the photomechanical response of glassy, azobenzene-functionalized polyimides, Macromolecules 47 (2014) 659–667.
[27] S.D. Kim, S. Lee, J. Heo, S.Y. Kim, I.S. Chung, Soluble polyimides with trifluoromethyl pendent groups, Polymer 54 (2013) 5648–5654.
[28] J. Ishii, A. Takata, Y. Oami, R. Yokota, L. Vladimirov, M. Hasegawa, Spontaneous molecular orientation of polyimides induced by thermal imidization (6). Mechanism of negative in-plane CTE generation in non-stretched polyimide films, Eur. Polym. J. 46 (2010) 681–693.
[29] G. Song, X. Zhang, D. Wang, X. Zhao, H. Zhou, C. Chen, G. Dang, Negative in-plane CTE of benzimidazole-based polyimide film and its thermal expansion behavior, Polymer 55 (2014) 3242–3246.
[30] Z. Liu, Z. Mi, C. Chen, H. Zhou, X. Zhao, D. Wang, Preparation of hydrophilic and antifouling polysulfone ultrafiltration membrane derived from phenolphthalin by copolymerization method, Appl. Surf. Sci. 401 (2017) 69–78.
[31] K.M. Zia, A. Noreen, M. Zuber, S. Tabasum, M. Mujahid, Recent developments and future prospects on bio-based polyesters derived from renewable resources: a review, Int. J. Biol. Macromol. 82 (2016) 1028–1040.
[32] Y. Guan, D. Wang, G. Song, G. Dang, C. Chen, H. Zhou, X. Zhao, Novel soluble polyimides derived from 2,2′-bis[4-(5-amino-2-pyridinoxy)phenyl]hexafluoropropane: preparation, characterization, and optical, dielectric properties, Polymer 55 (2014) 3634–3641.
[33] L. Qingquan, T. Fuqiang, Y. Chun, H. Lijuan, W. Yi, Modified isothermal discharge current theory and its application in the determination of trap level distribution in polyimide films, J. Electrost. 68 (2010) 243–248.
[34] S. Xu, Y. Wang, Novel thermally cross-linked polyimide membranes for ethanol dehydration via pervaporation, J. Membr. Sci. 496 (2015) 142–155.
[35] V. Ratta, A. Ayambem, J.E. McGrath, G.L. Wilkes, Crystallization and multiple melting behavior of a new semicrystalline polyimide based on 1,3-bis(4-aminophenoxy)benzene (TPER) and 3,3′,4,4′-biphenonetetracarboxylic dianhydride (BTDA), Polymer 42 (2001) 6173–6186.
[36] L. Jasinska-Walc, D. Dudenko, A. Rozanski, S. Thiyagarajan, P. Sowinski, D. van Es, J. Shu, M.R. Hansen, C.E. Koning, Structure and molecular dynamics in renewable polyamides from dideoxy–diamino isohexide, Macromolecules 45 (2012) 5653–5666.
[37] S.-H. Hsiao, W. Guo, C.-L. Chung, W.-T. Chen, Synthesis and characterization of novel fluorinated polyimides derived from 1,3-bis(4-amino-2-trifluoromethylphenoxy)naphthalene and aromatic dianhydrides, Eur. Polym. J. 46 (2010) 1878–1890.
[38] S. Ando, T. Matsuura, S. Sasaki, Coloration of aromatic polyimides and electronic properties of their source materials, Polym. J. 29 (1997) 69–76.
[39] G. Hougham, G. Tesoro, J. Shaw, Synthesis and properties of highly fluorinated polyimides, Macromolecules 27 (1994) 3642–3649.
[40] G.A. Norton, S.L. Devlin, Determining the modern carbon content of biobased products using radiocarbon analysis, Bioresour. Technol. 97 (2006) 2084–2090.
[41] Y.-T. Chern, Low dielectric constant polyimides derived from novel 1,6-bis[4-(4-aminophenoxy)phenyl]diamantane, Macromolecules 31 (1998) 5837–5844.